Available online at www.sciencedirect.com

ScienceDirect

Mechanical Systems and Signal Processing 21 (2007) 2880–2899

Mechanical Systems and Signal Processing

www.elsevier.com/locate/jnlabr/ymssp

A multi-channel feedback algorithm for the development of active liners to reduce noise in flow duct applications

B. Mazeaud, M.-A. Galland*

Laboratoire de Mecanique des Fluides et d'Acoustique, UMR CNRS 5509, Ecole Centrale de Lyon, 69134 Ecully Cedex, France

Received 10 April 2006; accepted 10 February 2007
Available online 3 March 2007

Abstract

The present paper deals with the design and development of the active part of a hybrid acoustic treatment combining porous material properties and active control techniques. Such an acoustic system was developed to reduce evolutionary tones in flow duct applications. Attention was particularly focused on the optimization process of the controller part of the hybrid cell. A piezo-electric transducer combining efficiency and compactness was selected as a secondary source. A digital adaptive feedback control algorithm was specially developed in order to operate independently cell by cell, and to facilitate a subsequent increase in the liner surface. An adaptive bandpass filter was used to prevent the development of instabilities due to the coupling occurring between cells. Special care was taken in the development of such systems for time-varying primary signals. An automatic frequency detection loop was therefore introduced in the control algorithm, enabling the continuous adaptation of the bandpass filtering. The multi-cell structure was experimentally validated for a four-cell system located on a duct wall in the presence of flow. Substantial noise reduction was obtained throughout the 0.7–2.5 kHz frequency range, with flow velocities up to 50 m/s.

Keywords: Active noise control; Multi-channel architecture; Feedback algorithm; Frequency detection; Transmission loss

1. Introduction

This paper describes the complete design and development of the active part of a new kind of acoustic liner developed to reduce noise throughout a wide frequency range. Global control is employed in order to minimize the energy of the studied system, or the power it radiates. Passive means often become inadequate at low frequencies since they require a substantial thickness of material, usually incompatible with industrial requirements. Active control has amply proved its ability to solve some low frequency noise problems for which passive devices are ineffective. However, in the case of global control, the quantity to minimize is difficult to estimate in practice and an alternative can be found by reformulating the problem in terms of control of the boundary conditions. One can thus define the optimal impedance as that which has to be achieved on the physical boundaries of the system in order to minimize the relevant energetic index. The

*Corresponding author. Tel.: +33 04 72 18 60 13; fax: +33 04 72 18 91 43.
E-mail address: Marie-Annick.Galland@ec-lyon.fr (M.-A. Galland).

0888-3270/$ - see front matter
doi:10.1016/j.ymssp.2007.02.009

present work focuses on reducing the noise propagating in a flow duct, and in particular the time-varying tones existing in fan noise. The study was carried out in the context of the European SILENCER program (Significantly lower community exposure to aircraft noise GRD1-2000-25297), intended to design new technologies to attenuate perceived aircraft noise. It was therefore sought to reduce radiated power by achieving duct wall boundary conditions as close as possible to those obtained with the pre-determined optimal impedance (Sellen et al. [1]). The treatment presented here results from the connection of hybrid cells, each comprising a passive layer backed by an active noise control (ANC) system. The hybrid absorption concept refers to the simultaneous and dual operation of cells that are active at low frequencies and passive at higher frequencies. The objective was to yield a wall impedance that provides a maximum insertion loss throughout a larger frequency range than do existing acoustic liners.

The hybrid structure was selected since it presents many advantages. Direct active control of impedance is quite difficult to implement because it requires that the impedance be measurable. Many studies have been devoted to the development of such systems and cannot all be cited here. Only a brief outline of the various strategies drawn up will be given. Many studies involved a two-microphone probe to extract the impedance or the reflection coefficient. The first developments were for air applications, by Guicking et al. [2] and later Orduna et al. [3]; others were devoted to underwater acoustics applications (see Howard et al. [4]). Another possibility for obtaining a surface impedance is to use directly the acoustic velocity estimated from a specific sensor, such as an accelerometer fixed on the secondary source, in addition to the pressure measured in the vicinity: see Nicholson et al. [5] and Furstoss et al. [6]. However, both strategies involve a limited frequency range (inherent in the sensors), and require effective control of two signals. An alternative strategy consists in using an absorbent material to simplify the control system. Olson and May [7] first suggested using their "electronic sound absorber" behind a resistant cloth, to build an active absorber. Guicking et al. [8] carried out the first experimental investigations on the subject. Later, our team applied adaptive algorithms to achieve active control of the real part of the impedance (Furstoss et al. [6]). Subsequent studies focused on the development of this technology for flow duct and nacelle applications [9–12]. Thanks to the double functioning mode of the resulting hybrid cells, the frequency bandwidth over which the efficiency is high is enlarged with respect to conventional passive treatments and purely active technologies. The design of the passive part, which has to be performed for each considered application, is detailed in Sellen et al. [1].

If a substantial minimum is targeted, one needs, in many applications, to cover a large surface. Extended smart liners are obtained by connecting several individual cells, rather than by extending the cell size, for reasons of pressure uniformity at the rear face of the porous layer. The cell size is thus related to the wavelength in question. A multiple-input/multiple-output (MIMO) control system is therefore necessary to enlarge active surfaces. Digital MIMO ANC feedforward systems proved to be particularly efficient for the control of periodic noise as reported by Galland et al. [9] in experiments using a four-cell prototype. Memory requirements and computation loads, however, quickly become limiting factors when, for instance, time-varying periodic noise is being considered. Moreover, in the targeted final application, such as turbojet inlet coverings, a reference signal synthesized from the engine speed may be insufficiently correlated with the perturbation for the noise level to be able to be greatly reduced. Thus, feedback control is preferable. Analogue feedback controllers were developed and tested, but with poor results because their design mainly depended on the electro-acoustic response of each cell (Galland et al. [9]). As discrepancies always occur in the manufacturing of the cells, an individual control filter has to be designed for each of them. Moreover, changes in the environment often require changing the control filter response, which cannot be easily done with an analogue filter. Thus, independent active cells with auto-adaptive feedback digital controllers should be the ideal system for extending the treated area in industrial applications. MIMO ANC feedback systems have essentially been developed for vibro-acoustic transmission problems. In these cases, the controller, even if not adaptive, can remain efficient in spite of discrepancies between acoustic plants. It should be noted that adaptive systems capable of generating large-scale smart surfaces do not really exist at present. We here report an original ANC system allowing adaptive "cell-by-cell" feedback control for tones. We also propose a particularly interesting enhancement for turbojet inlet applications, which enables non-stationary periodic perturbations to be dealt with.

The paper is structured as follows. Section 2 describes the hybrid cell and includes a brief report on the main conclusions concerning the actuator design. The following sections deal with the controller in greater detail.

Section 3 presents the single-channel structure. Then, the extension from single to multi-channel is reported in Section 4. Section 5 gives the analysis of the proposed algorithm, which is coupled to a multi-tone frequency tracking system in Section 6. Lastly, experimental validations are presented in Section 7. Section 8 concludes the paper.

2. Description of the hybrid cell

2.1. Principle

The basic principle of the active liner as first introduced by Olson and May [7] can be summarized as follows: at low frequencies, the acoustic behavior of a porous layer of thickness e is mainly described by the flow resistivity σ of the material. For a plane wave impinging on a porous sample under normal incidence as shown in Fig. 1(a):

$$\sigma = \frac{p_1 - p_2}{ev}, \tag{1}$$

with p_1, p_2, and v the acoustic pressures and velocity. If the pressure vanishes at the back face, that is $p_2 = 0$, the layer input impedance Z_S becomes equal to the flow resistance of the material sample σe. Under normal incidence, total absorption is obtained when this impedance matches the characteristic impedance of air $Z_0 = \rho_0 c_0$ where ρ_0 is the air density and c_0 the sound velocity. This fundamental property is used when designing passive "$\lambda/4$ absorbers" (cf. Fig. 1(b)). By positioning the material at a distance equal to one quarter of a wavelength from the rigid wall, this boundary condition can be reproduced. However, such a technique raises two major problems. First, the required air gap for a low frequency is incompatible with industrial constraints (e.g., $\lambda/4 = 0.17$ m in air at 500 Hz). Then, the efficiency of such a system is limited to narrow frequency bands. Active control techniques appear to be particularly efficient in avoiding these drawbacks: the air gap can be replaced by an active control loop which minimizes the pressure (cf. Fig. 1(c)). Hence, broadband absorption can be achieved with a reduced absorbent thickness. This method also offers the advantage of separating the control system from a hostile environment (air flow or hot stream for instance).

2.2. Adaptation to aeronautics applications

The first active cells we studied used glass wool as the porous layer and an electro-dynamic loudspeaker as the secondary source. Adaptation to aeronautics applications led us to completely change both passive and active parts. The actuator development was carried out in collaboration with Metravib RDS (Hilbrunner et al. [10]).

The cell cross-section (55 mm × 55 mm) was chosen to ensure uniform pressure on the back face of the porous layer throughout the whole frequency range (0.5–2.5 kHz). Pressure was reduced by active control on a single point corresponding to the position of the control microphone. The efficiency of the active cell thus depended on the effective extent of the low pressure area behind the porous layer. Theoretical and experimental investigation confirmed that the center of the cross-section was the best position for that.

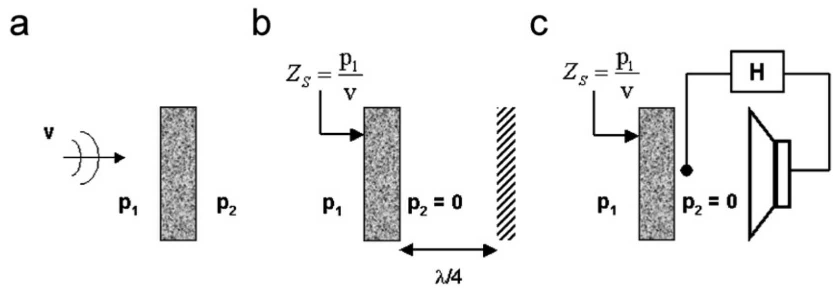

Fig. 1. Hybrid absorption principle: (a) low frequency approximation, (b) $\lambda/4$ resonator, and (c) active control.

The technological choice finally turned to piezo-electric ceramics, lighter and more compact than classical loudspeakers. The basic principle consists in exciting a multi-layer plate in a flexural (bending) deformation mode. In our case, for the sake of efficiency, one ceramic was used on each face of the central aluminum plate, in an asymmetric (phase opposition) manner. It involved the presence of a back cavity in addition to the front cavity which is the air gap inherent in the passive functioning. It does not affect the behavior of the vibrating plate. For aeronautics applications, classical passive absorbents often become ineffective for frequencies below 2.5 kHz, and the active absorber has to be designed to deal with this frequency range. The piezo-electric transducer was optimized with two main objectives: to obtain high pressure levels throughout the frequency range of interest, and to improve controllability. Ideally, a non-resonant transducer should have been developed to simplify control loop processing, but it appeared that the requested acoustic levels (up to 150 dB on some harmonics) might not be reached without introducing a resonant frequency in the band of interest. The compromise adopted was to introduce a single resonance in the center of the frequency range to reach high radiated acoustic pressures, and to prevent the contribution of higher order modes that would introduce instabilities in the control loop by shifting the ceramic position away from the central position.

In the same way, classical porous material was replaced by resistive layers such as wire meshes, more suited to aeronautics applications. They also proved their ability to achieve a close-to-target impedance throughout a very large frequency range. This impedance is theoretically predetermined to produce the best noise reduction when applied to these applications. The optimization study on the passive part (Sellen et al. [1]) enabled the best-suited wire mesh to be selected. The most efficient liner was obtained with active functioning of the hybrid cell below 1.8 kHz and passive functioning above, the actuator plate then behaving as a rigid wall. The distance between the resistive layer and the plate was set at 20 mm.

The resulting elementary hybrid cell is represented in Fig. 2. The cavity on the back face of the actuator prevents the secondary source from radiating in that direction.

3. Presentation of the single-channel architecture

The basic idea of a digital feedback controller is to estimate the primary noise at the error sensor and to use it as the reference signal for the ANC filter. The use of an internal model control (IMC, Morari et al. [13]) feedback configuration enables feedforward control through the filtered-x least mean squares (FXLMS) algorithm. This is the concept behind the IMC-FXLMS algorithm.

3.1. Algorithm structure

The FXLMS algorithm is a modification of the standard LMS algorithm employed in feedforward control, to meet the need to include the effects of the unknown acoustic secondary-path transfer function $S(z)$ between the secondary source and the error sensor by modeling it with an additional finite-impulse-response (FIR) filter $\hat{S}(z)$. This algorithm is consequently widely used in ANC applications.

The IMC architecture is based on a reference signal regeneration technique whereby the secondary signal is filtered by $\hat{S}(z)$ and then subtracted from the error signal to generate an estimation of the primary noise. This

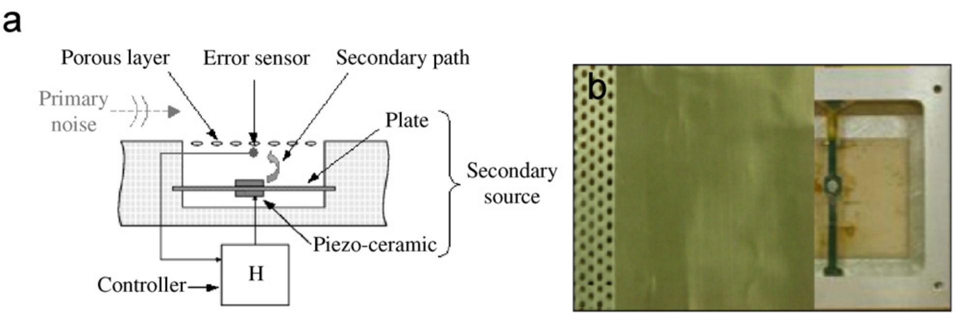

Fig. 2. The hybrid cell: (a) diagram, and (b) prototype (presence of a perforated grid necessary for nacelles manutention).

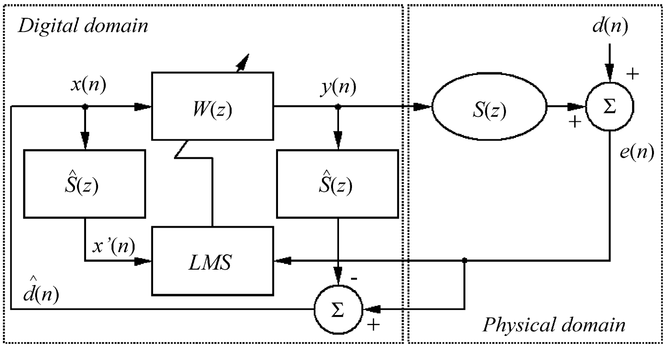

Fig. 3. The IMC-FXLMS architecture.

reference signal is then used as input by the ANC filter. The complete single-input/single-output (SISO) adaptive feedback system using the IMC-FXLMS algorithm is illustrated in Fig. 3.

$d(n)$ represents the primary signal, $x(n)$ its regeneration from the error signal $e(n)$, and $y(n)$ the output of the control filter $W(z)$. It should be noticed that off-line modeling (the so-called identification stage) is performed before the control stage to obtain the secondary-path estimate $\hat{S}(z)$, which is fixed thereafter. The reader is referred to Elliott's textbook [14] for further details on implementing the steepest-descent gradient algorithm.

3.2. Algorithm analysis

The error signal obtained at the error sensor can be expressed in the z-domain as

$$E(z) = D(z) + S(z)Y(z). \tag{2}$$

Since

$$Y(z) = W(z)X(z) = W(z)[E(z) - \hat{S}(z)Y(z)], \tag{3}$$

that is

$$Y(z) = \frac{W(z)E(z)}{1 + \hat{S}(z)W(z)}. \tag{4}$$

The foregoing Eq. (2) can be rearranged as

$$E(z) = D(z) + S(z)\left[\frac{W(z)E(z)}{1 + \hat{S}(z)W(z)}\right]. \tag{5}$$

This can also be recast as

$$E(z) = \frac{D(z)[1 + \hat{S}(z)W(z)]}{1 + [\hat{S}(z) - S(z)]W(z)}, \tag{6}$$

and the overall transfer function $H(z)$ from $d(n)$ to $e(n)$ of the adaptive feedback ANC structure shown in Fig. 3 is therefore,

$$H(z) = \frac{E(z)}{D(z)} = \frac{[1 + \hat{S}(z)W(z)]}{1 + [\hat{S}(z) - S(z)]W(z)}. \tag{7}$$

Assuming that the secondary-path model is perfect (i.e. $\hat{S}(z) = S(z)$), the algorithm consists in removing the feedback contribution so that $x(n) = d(n)$. In fact, the control filter $W(z)$ performs as a feedforward controller, with $d(n)$ being both the reference signal and the unwanted disturbance, and is therefore internally stable.

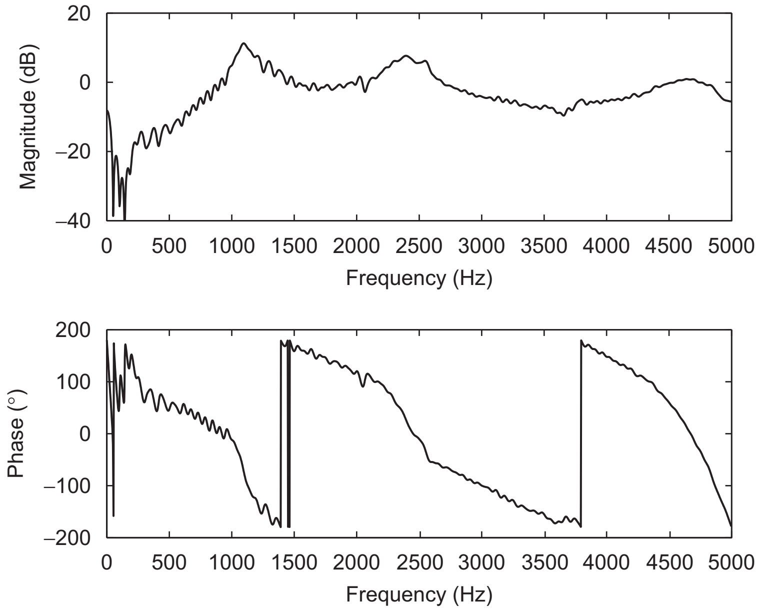

Fig. 4. The measured frequency response of the hybrid cell.

3.3. Algorithm performance

Fig. 4 shows the frequency response function (FRF) of the secondary-path measured with the I-deas® data acquisition system. The hybrid cell was mounted on the inner wall of a duct (cf. Section 7.1 for the experimental configuration). The sampling frequency was set to 10 kHz. This response is characteristic of the piezo-electric transducer technology used here, i.e. of a resonant actuator. As mentioned in Section 2, it was optimized to yield high gain at the center of the frequency range of interest, close to 1.1 kHz. In the following, the secondary-path model is supposed to be perfect.

The optimal control filter $W^{\mathrm{opt}}(z)$, that is to say the filter that ensures the zero-pressure condition at the control microphone ($E(z) = 0$ in Eq. (7)), is given by

$$W^{\mathrm{opt}}(z) = -\frac{1}{\hat{S}(z)}. \tag{8}$$

This inversion results in a non-causal filter (its phase increasing with respect to frequency). The performance of the IMC-FXLMS algorithm therefore depends on the predictability of the primary noise. Controlling any periodic disturbances or narrowband noise is thus quite feasible. In contrast, it would be pointless to seek to control a random broadband noise.

For instance, we simulated the control of a 1.25-kHz single sine wave as primary noise. In such a configuration, a two-tap control filter is sufficient to approximate the function $-1/S(z)$ (one value for the magnitude and one for the phase). Fig. 5 shows a FRF plot of the ideal and two-tap calculated control filters. Since these two curves intersect exactly at 1.25 kHz, the control is necessarily optimal, with a maximum level of noise reduction being achieved at the error sensor.

Increasing the order of the control filter creates a bandpass filtering effect around the frequency of the primary noise, as presented in Fig. 5 for a 20-tap filter. This property takes on importance with an additional random broadband noise perturbation, since a selection of the necessary information comes about. Furthermore, a low-order filter acts as an all-pass filter and can therefore make control more difficult.

The robustness of such a feedback algorithm has been extensively discussed in the literature [15–17]. It emerges that the SISO structure provides rapid and stable multi-tone convergence in noise signals, without increasing the random noise. It works similarly to the classical feedforward FXLMS algorithm, but

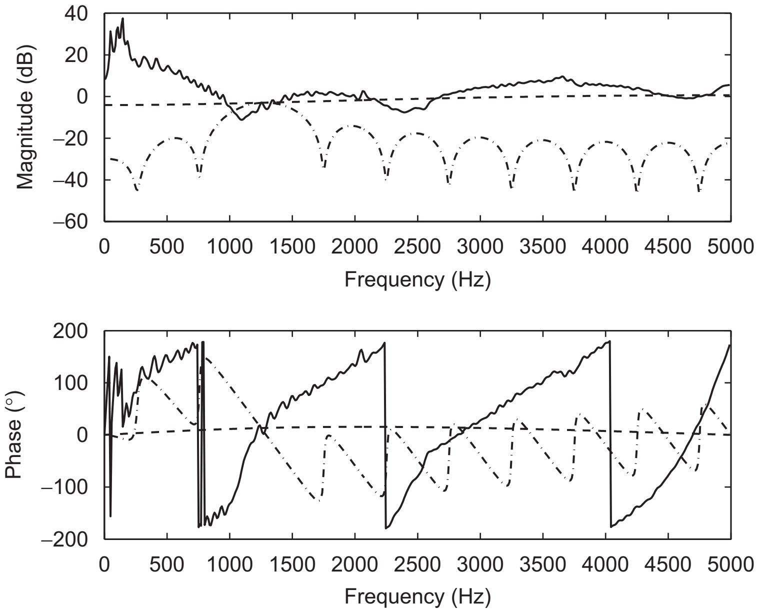

Fig. 5. Ideal and calculated control filter (solid line: ideal control filter; thin line: 2-tap calculated control filter; dash-dot line: 20-tap calculated control filter).

with the sizeable advantage of requiring only one input. However, the IMC-FXLMS algorithm is more sensible to a change in the secondary path because it also impacts on the definition of the reference signal.

4. Extension to the multi-channel case

Larger surfaces are obtained by assembling several cells, which form a hybrid liner. Interactions then appear between cells, since each error sensor picks up the sound waves emitted by all the secondary sources. This section presents how such cross-paths have to be taken into account in ANC applications, in addition to the direct secondary paths.

Most of the related studies (Elliott [19], Kuo et al. [20]) present a multi-channel architecture that estimates the primary noise at each error sensor. This is a multi-reference algorithm in the sense that, in a $K \times K$ configuration (K secondary sources and K error sensors), K reference signals must be synthesized and the feedback controller is represented by a $K \times K$ matrix—the coefficients of which are the adaptive FIR filters $(W_{ij}(z))_{i,j=1\ldots K}$. Thus, each secondary source controls its own influence on each error sensor.

Significant attenuations are obtained with these multi-channel adaptive feedback ANC systems for small values of K. But it emerges from all these experiments that real-time developments are often limited for configurations requiring a large number of channels, since the computation complexity and memory costs grow with the number of cross-paths. A simplified version of this algorithm is built in this section, with the objective of showing and explaining through an example that the MIMO case cannot be deduced straightforwardly from the SISO case.

4.1. The simplified IMC-MFXLMS algorithm

In order to avoid the problem of subsequent computational loads, cross-path contributions are ignored in the reconstruction of the references and in the adaptation of the control filters' coefficients. Thus, a simplified version of the algorithm is obtained, in which only the self and main feedback produced by each cell is removed (see Fig. 6). The cross-contributions are then seen as part of the signal to be minimized. The interest

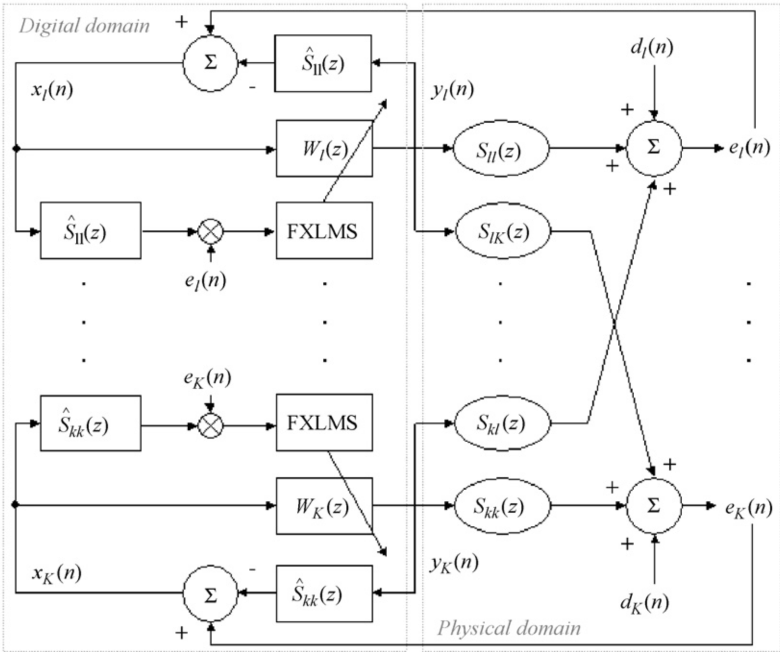

Fig. 6. Detailed block diagram of the simplified $K \times K$ IMC-MFXLMS algorithm.

of such a structure for real-time applications must be underlined once again; when large numbers of cells are considered, only K secondary-paths are taken into account in the digital domain instead of K^2. Moreover, the matrix of feedback controllers amounts to the diagonal matrix $(W_{ii}(z))_{i=1\ldots K}$. However, even if cross-contributions are ignored in this new architecture, they still exist in the physical domain and instabilities can therefore arise.

4.2. Structure analysis

Assuming perfect modeling of the direct paths, the reference signal at each error sensor j is obtained with the following equation:

$$X_j(z) = E_j(z) - S_{jj}(z)Y_j(z) = E_j(z) - S_{jj}(z)W_j(z)X_j(z). \tag{9}$$

It is to be noted that in this MIMO structure, the optimal control filters are expressed in the same way as in SISO systems, since Eq. (9) shows that they depend only on the direct paths.

The measured error signal is

$$E_j(z) = D_j(z) + \sum_{i=1}^{K} S_{ij}(z)Y_i(z) = D_j(z) + \sum_{i=1}^{K} S_{ij}(z)W_i(z)X_i(z), \tag{10}$$

and Eq. (9) can thus be recast as

$$X_j(z) = D_j(z) + \sum_{\substack{i=1 \\ i\neq j}}^{K} S_{ij}(z)W_i(z)X_i(z). \tag{11}$$

Finally, in matrix notation and after N iterations, the reference signal can be expressed as follows:

$$\mathbf{X} = \mathbf{G}_N\mathbf{D} + \mathbf{M}^{N+1}\mathbf{X}, \tag{12}$$

where $\mathbf{G}_N$ is a geometric series with a ratio of $\mathbf{M}$, $\mathbf{X}(z) = [X_1(z) \cdots X_K(z)]^{\mathrm{T}}$ and $\mathbf{D}(z) = [D_1(z) \cdots D_K(z)]^{\mathrm{T}}$ are the vectors of reference and error signals respectively, and

$$\mathbf{M} = \begin{pmatrix} 0 & W_2 S_{21} & \cdots & W_K S_{K1} \\ W_1 S_{12} & 0 & & \vdots \\ \vdots & & \ddots & \vdots \\ W_1 S_{1K} & \cdots & \cdots & 0 \end{pmatrix}. \tag{13}$$

Thus, the convergence of the process (and therefore the overall system stability) depends on the eigenvalues of $\mathbf{M}$ and intrinsically on the cross-paths. The induced necessary and sufficient stability condition is that the eigenvalues $(\lambda_i)_{i=1\dots K}$ must have moduli that are strictly less than unity. This condition does not, in general, admit a trivial characterization in terms of cross secondary-paths as well as control filters.

Indeed, the 2×2 architecture seems to be the only one for which the expression of the stability condition is physically interpretable. In that case, the direct secondary paths have to be jointly greater in amplitude than the cross-paths throughout the whole spectrum. This criterion can be generalized to the MIMO case, but it becomes a sufficient condition of stability only (Leboucher et al. [21]).

4.3. Structure performance

The control of a 1.25-kHz tone in noise perturbation (SNR = 15 dB) is taken as an example, in the 4×4-system case. The evolution of the maximal eigenvalue (in modulus) versus frequency is represented in Fig. 7 (solid line). The M matrix has been determined from the optimal control filter in this case. The necessary and sufficient stability criterion is not fulfilled for the IMC-MFXLMS algorithm, at the primary frequency and around the main resonances of the piezo-electric transducer: 1.1, 2.4 and 4.5 kHz. This behavior is confirmed in Fig. 8, which gives the spectra with and without control at one of the error sensors. An increase in noise is observed at the main instability frequencies, i.e. for the highest values of the maximum eigenvalue.

Acoustic coupling occurring between the cells can thus produce instabilities at some frequencies, resulting in overall instability.

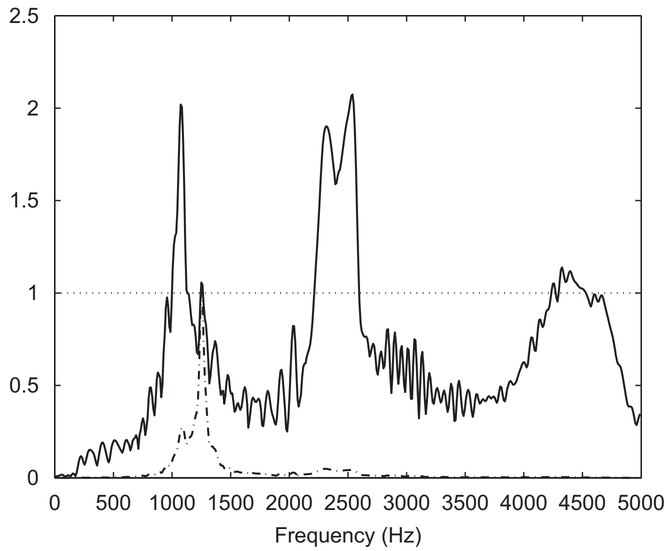

Fig. 7. Optimal eigenvalues obtained for a 1.25-kHz tone as primary perturbation (solid line: with the IMC-MFXLMS; dash-dot line: with the IMC-MDFXLMS).

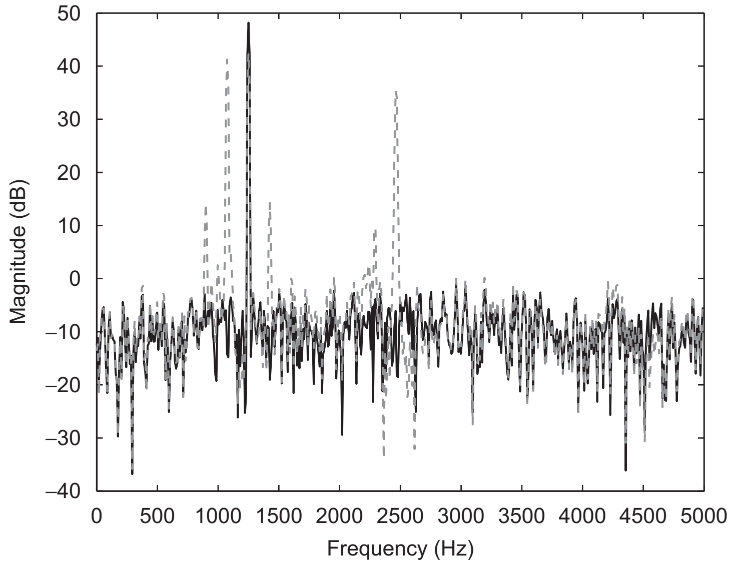

Fig. 8. IMC-MFXLMS algorithm instabilities (solid line: without control; dashed line: with control).

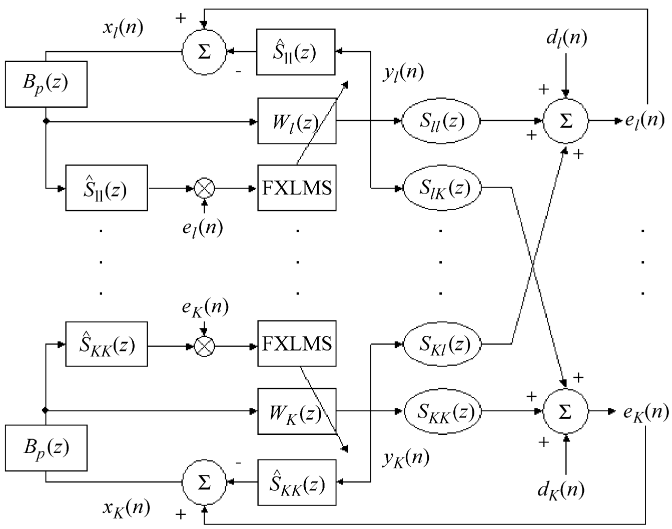

Fig. 9. Detailed block diagram of the IMC-MDFXLMS algorithm including the bandpass filters Bp.

5. Improvement of the multi-channel system

This section presents a robust solution that is efficient in real-time applications.

5.1. The IMC-MDFXLMS algorithm

The novel idea is to improve stability by filtering each reference signal by means of an adaptive bandpass filter. This filtering is carried out in a band located around the sinusoidal frequency of the primary noise. The compulsory condition is to have both zero magnitude and phase at the central frequency in order to implement a viable control. This algorithm was named IMC-MDFXLMS for IMC Mimo Diagonalized FXLMS. Fig. 9 presents a block diagram of this MIMO adaptive feedback ANC structure with $B_p(z)$ as the bandpass filter. This filtering plays a part in the expression of the optimal control filter inherent in each cell since it is henceforth equal to, for $i = 0...K$:

$$W_i^{\mathrm{opt}}(z) = -\frac{1}{S_{ii}(z)B_p(z)}. \tag{14}$$

The addition of the bandpass filters has the effect of reducing the eigenvalues close to zero everywhere but at the central frequency (see Fig. 7, dotted line). For that particular frequency, it can be proven that the use of the optimal filters as control filters prevents potential instabilities from developing, since all error signals are equal to zero (see Eq. (7)). Finally, all instabilities may be reduced by bandpass filtering. Only low-order bandpass filters have to be considered, because the larger the order the steeper the phase jump around the central frequency of the bandpass filter; and this phase jump must be as small as possible, so that a slight frequency variation between the central frequency of the bandpass filter and that of the reference signal will not have too negative an impact on the noise control. Three numerical bandpass filters are widely used: the Butterworth, Chebyshev and Elliptic filters. For second-order filters, their specifications are very close, or indeed identical in the case of the Chebyshev and Elliptic filters. This filtering gives satisfactory control when applied to MIMO ANC systems. If the ANC algorithm has to deal with several sinusoids, several bandpass filters can be used in parallel, each centered around one of the frequencies to be processed. The proposed algorithm is also adapted to the specific hybrid operation. As suggested by Sellen et al. [1], only the sinusoidal components below the cut-off frequency of approximately 1.8 kHz have to be reduced, whereas a zero-velocity boundary condition has to be ensured at the actuators for the other tones. If no bandpass filtering is executed for frequencies above 1.8 kHz, these frequencies will therefore be ignored by the control algorithm.

5.2. Algorithm performance

To get a clearer picture on that particular behavior, the case of a three-tone-in-noise (SNR = 15 dB) excitation is examined. Two tones are below the cut-off frequency and must therefore be controlled by the ANC algorithm (1000 and 1500 Hz). The remaining tone has to be reduced thanks to the passive functioning (2000 Hz). To this aim, the IMC-MDFXLMS algorithm is outfitted with two parallel Butterworth bandpass filters, with a 100-Hz −3 dB bandwidth, centered around 1000 and 1500 Hz. Control is started at $t = 1$ s. In contrast to Fig. 8, Fig. 10 shows the satisfactory behavior of the algorithm. Ten coefficients per control filter are sufficient to ensure rapid convergence and stability. This is a decisive advantage of bandpass filtering because, in addition to saving memory space, the convergence time was often observed to be shorter for MIMO systems with low-order control filters.

However, all these filters are fixed and pre-calculated from the knowledge of the tones to be controlled. This is a disadvantage for the application under consideration, since the algorithm has to deal with time-varying tones related to the fan engine rating.

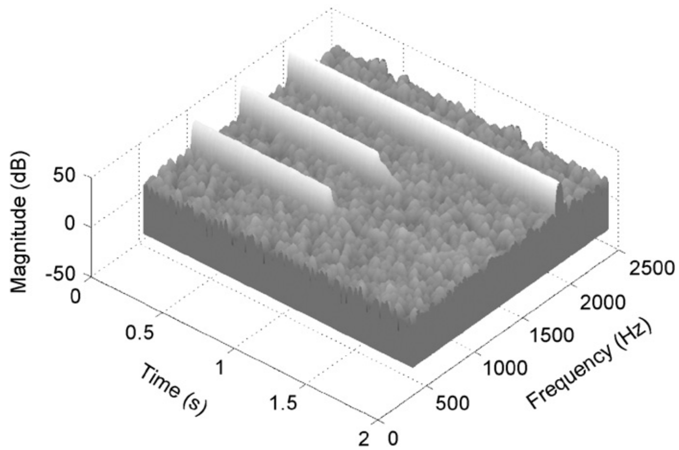

Fig. 10. Performance of the IMC-MDFXLMS algorithm on a three-sinusoid perturbation (1000, 1500 and 2000 Hz). Control on at 1 s.

6. Multi-tone ANC with self-adaptive bandpass filters

The numerical simulations have so far been run with given primary perturbation frequencies. However, in the final applications, these frequencies are taken to be unknown and it is therefore essential to develop a frequency detection system that, coupled with the proposed MIMO algorithm, will provide a totally self-sufficient ANC structure. But first, an adaptive bandpass filter easily tunable to follow the frequency evolution of the primary noise has to be found.

6.1. The adaptive line enhancer

Its basic principle is that of the adaptive notch filters (ANFs, Regalia [22]), expressed by the lattice formulation.

ANFs are infinite impulse response (IIR) filters generally used to filter out sine wave components with unknown frequencies immersed in broadband noise. They have a unit gain at all frequencies except at the sine wave frequencies where their gain is zero. Second-order ANFs in lattice form, as proposed by Regalia [22], are expressed by the following equation:

$$N_i(z) = \frac{A_i(z^{-1})}{A_i(\rho z^{-1})} = \frac{1 + a_i(n)z^{-1} + z^{-2}}{1 + \rho a_i(n)z^{-1} + \rho^2 z^{-2}}, \tag{15}$$

where ρ is the bandwidth factor (close to but less than unity) and $a_i(n) = -2\cos(\omega_i(n))$ is the notch frequency. Their advantages lie in the ease of controlling the bandwidth and in the intrinsic adaptivity, since an adaptive coefficient a_i commands the notch filter frequency adjustment. The -3-dB bandwidth is given by $B = 2\tan^{-1}((1-\rho)/1+\rho)$ (Regalia et al. [23]).

In our application, the purpose is to retrieve sinusoidal components from the reference signal, and bandpass filters complementary to ANFs are therefore considered. These filters are called adaptive line enhancers (ALE) and were first suggested by Widrow et al. [24]. For a given angular frequency ω_i, this therefore results in a second-order lattice-based filter, expressed as

$$B_p(z) = \frac{1-\rho}{2}\frac{1 - z^{-2}}{1 + ((1+\rho)/2)a_i z^{-1} + \rho z^{-2}}. \tag{16}$$

It should be noted that for $\rho = 0.97$ (50-Hz bandwidth), the resulting filter gives approximately the same frequency response as the aforementioned bandpass filters.

6.2. The multi-tone frequency tracking system

Let $r(n)$ be a p-sinusoid in noise signal, that is,

$$r(n) = s(n) + t(n), \tag{17}$$

where $s(n) = \sum_{i=1}^{p} U_i \cos(\omega_i(n)n + \phi_i)$ and $t(n)$ is a zero-mean broadband noise with unknown variance. $(\omega_i(n))_{i=1\ldots p}$ $(0<\omega_i<\pi)$, $(U_i)_{i=1\ldots p}$ and $(\phi_i)_{i=1\ldots p}$ denote the unknown angular frequencies, amplitudes and phases, respectively. $(\omega_i(n))_{i=1\ldots p}$ are the time-varying parameters to be determined. The frequency detection algorithm is based on the recursive least squares (RLS) method applied to second-order ANFs in a cascaded structure.

6.2.1. The ANF cascaded structure

The basic concept of ANFs in a cascaded structure (ANF^C) is to put p ANFs in series so that the frequency components of the p-sinusoid signal are notched one by one. Such a frequency decoupling property has been extensively discussed in the literature [25,26]. Each section of the cascade is adapted iteratively with its output, the error function $\varepsilon_{i+1}(n)$, until this comes to comprise one sinusoid fewer plus the slightly filtered background noise. Finally, the global notched signal comes to approximate the broadband noise. The block diagram of such an architecture is presented in Fig. 11.

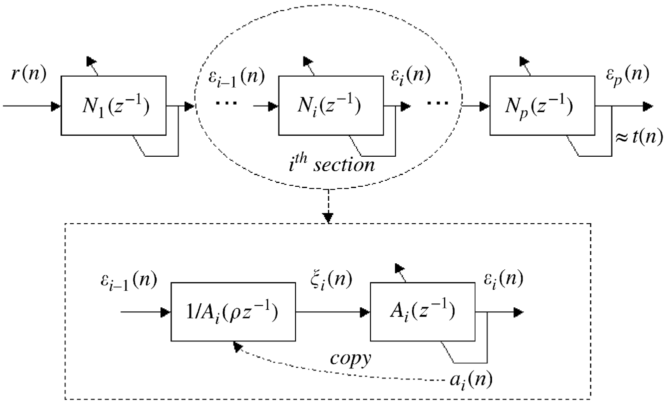

Fig. 11. Block diagram of cascade second-order ANFs.

6.2.2. Frequency tracking principle

The objective is to find the time-varying notch frequencies $(a_i(n))_{i=1\ldots p}$ thanks to an adaptive algorithm. The idea that underlies the frequency detection system is to use the simple recurrence

$$A_0(z^{-1})u(n) = 0, \tag{18}$$

verified for the signal $u(n) = \cos(\omega_0 n + \phi_0)$, in such a way as to determine the fixed notch frequency $a_0 = -2\cos(\omega_0)$. On this basis, the quantity to minimize will necessarily be connected to the function $A_i(z^{-1})\varepsilon_{i-1}(n)$ for each time-varying sinusoid. More precisely, this minimization should be applied to the so-called prediction error function $\varepsilon_i(n)$ obtained with the enhanced noiseless signal $\xi_i(n)$ filtered by $A_i(z^{-1})$, where $\xi_i(n)$ is defined as follows:

$$\xi_i(n) = \frac{1}{A_i(\rho z^{-1})}\varepsilon_{i-1}(n). \tag{19}$$

Indeed, the IIR filter $1/A_i(\rho z^{-1})$ acts as a line enhancer, thus weakening the influence of noise on the frequency detection system and allowing a frequency component of the $(p-i+1)$-sinusoid signal to be arbitrarily selected. The estimation procedure uses the RLS scheme proposed by Haykin [27] to compute this minimization. The cost function is defined as the sum of exponentially weighted least squares:

$$\mathscr{E}_i = \sum_{l=1}^{n} \lambda^{n-l}|A_i(z^{-1})\xi_i(l)|^2, \tag{20}$$

where λ is called the ‘‘weighting factor’’ and represents a positive constant close to but less than unity. Finally, the most recent prediction filter coefficients $((a_i(n))_{1\ldots p})$ are used to update the coefficients of the IIR section.

λ and ρ are exponentially updated thanks to the time-recursive form

$$\begin{cases} \lambda(n) = \lambda_0\lambda(n-1) + (1-\lambda_0)\lambda_\infty, \\ \rho(n) = \rho_0\rho(n-1) + (1-\rho_0)\rho_\infty, \end{cases} \tag{21}$$

in order to reduce convergence time.

Travassos et al. [28] first suggested this kind of decomposition into a transversal section cascaded with an IIR section. Later developments were proposed by Kim et al. [29].

6.3. Multi-tone track and control algorithm performance

The basic principle of this ANC system is to use the coefficients $(a_i(n))_{1\ldots p}$ calculated by the cascaded frequency tracking system (ANF^C) and to copy them, for each sample time, in the p-ALEs in parallel (ALE^P) as suggested in Fig. 12. This thus provides multi-bandpass filtering reacting to the slightest change in the

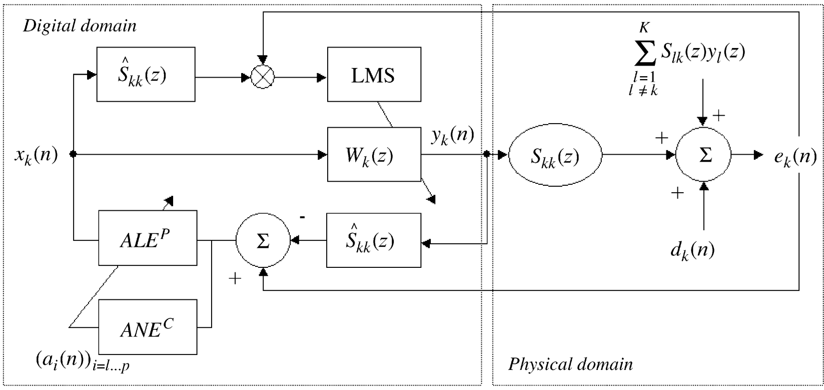

Fig. 12. Block diagram of the kth section of the IMC-MDFXLMS coupled with the frequency tracking system.

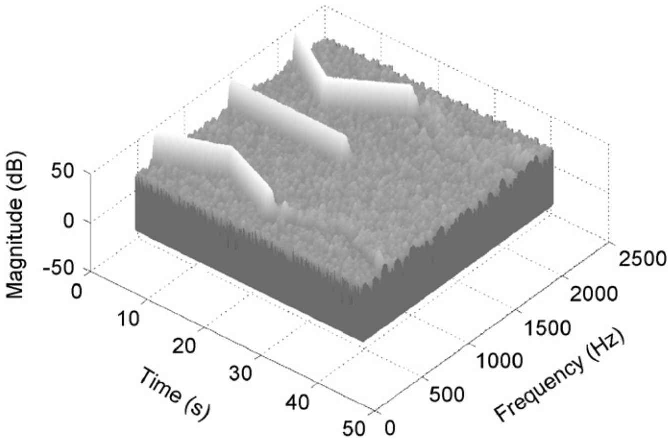

Fig. 13. Performance of a multi-tone track and control algorithm. Control on at 20 s.

primary perturbation. This ANC architecture only needs K inputs to perform this multi-tone track and control function. In order to examine the performance of such an architecture, a three-tone in noise excitation (SNR = 15 dB) was considered. This was composed of a fixed tone at 1.4 kHz and two time-varying sinusoids with rates of frequency change of 20 Hz/s (0.7–0.9 kHz) and 30 Hz/s (2.2–1.9 kHz), respectively. The order of each control filter was increased up to 20. λ_0 and ρ_0 were set at 0.99 whereas λ_∞ and ρ_∞ were worth 0.995. Fig. 13 illustrates a waterfall plot of the error signal at one of the error sensors with and without control (control on at 20 s). The result of the frequency estimation is given in Fig. 14. Adjustment to the right frequencies takes less than 150 ms. All the simulations run with the proposed algorithm showed good effectiveness, satisfying robustness and fast tracking capabilities.

7. Experimental validation

7.1. Presentation of the experimental laboratory setup

The MATISSE flow duct presented in Fig. 15 consists of a square cross-section duct (66 mm × 66 mm) with an axial length of approximately 3.20 m. It involves a large plane wave analysis domain up to about 2.5 kHz. The primary acoustic source is placed on the upper wall of the duct, downstream from the quiet flow generator system which allows the generation of a silent flow up to 50 m/s. An anechoic termination is ensured by an exponential outlet. Transmission loss (TL) measurements are carried out by a set of four flush-mounted microphones located up- and down-stream of the test section (Brüel & Kjær 1/4″ microphones $M_{i,i=1\ldots4}$) in

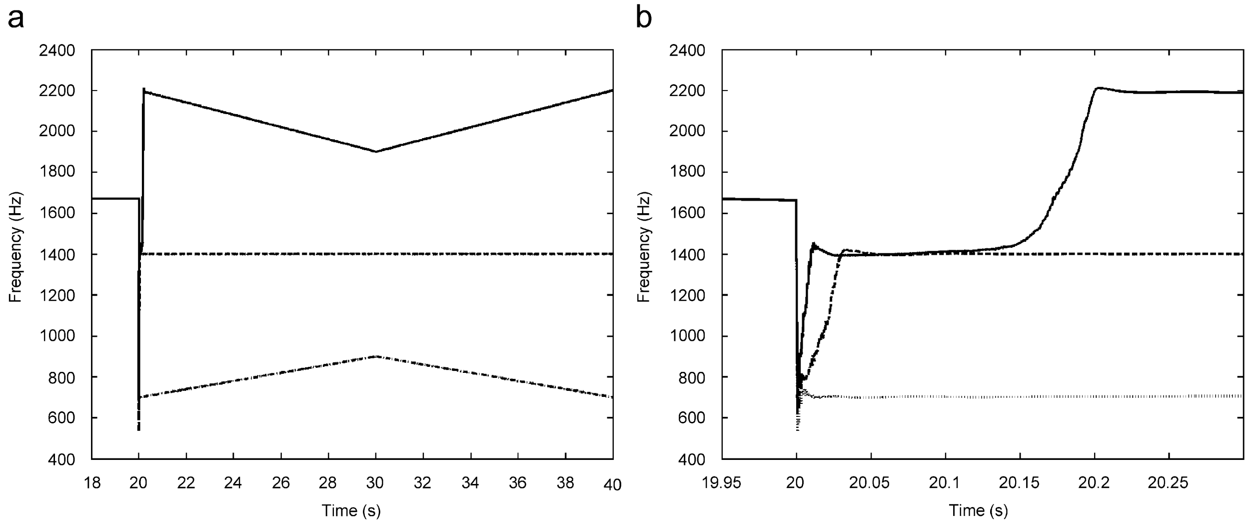

Fig. 14. Frequency tracking capabilities: (a) overall behavior, and (b) zoom on the very start of convergence.

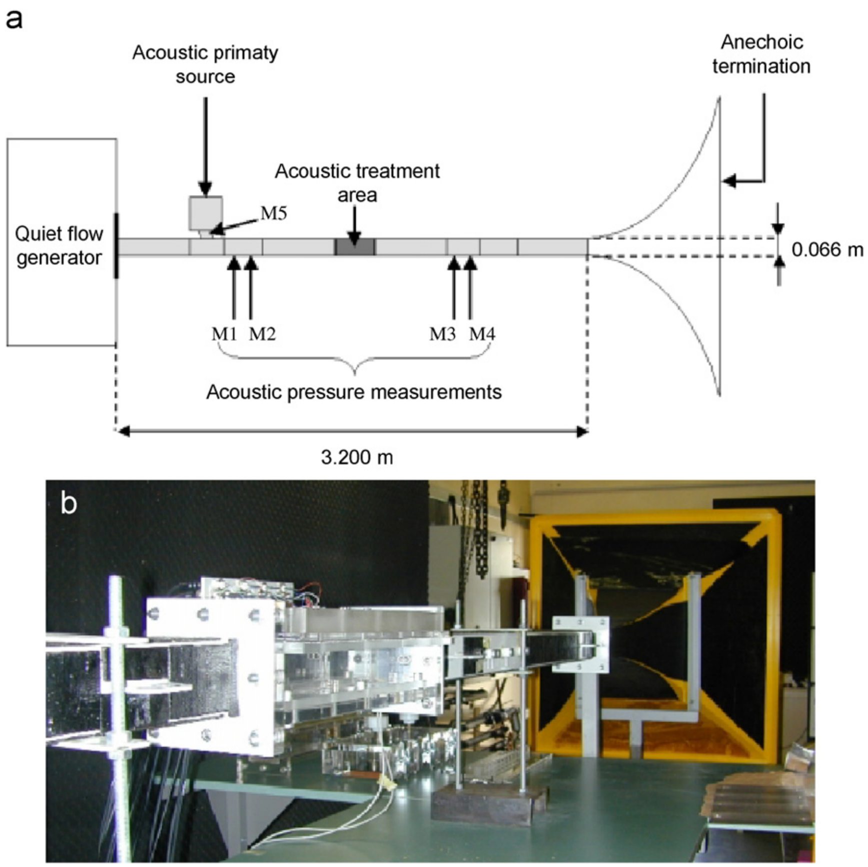

Fig. 15. The Matisse experimental facility: (a) schematic representation, and (b) test bench.

order to evaluate the performance of passive and active treatment. The liner is applied on the upper wall of the test section. It consists of a 220-mm long four-cell hybrid liner, as presented in Fig. 16. The reader is referred to [1] for an exhaustive description of the experimental setup and the choice of performance indexes.

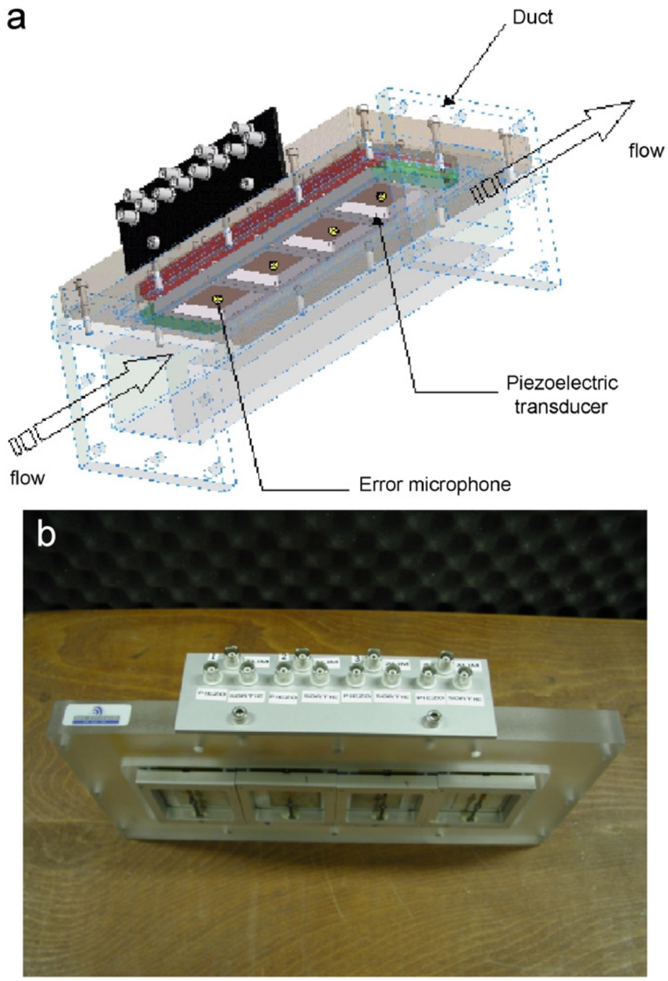

Fig. 16. The four-cell hybrid liner: (a) schema, and (b) prototype.

The control and filtering algorithms were first implemented with Simulink® and then downloaded onto a dSPACE-DS1103 controller board equipped with a TI-TMS320 floating-point DSP via the TI-F240 compiler and MATLAB/Real-Time-Workshop®. All acquisitions were made with a VXI data acquisition system piloted via I-DEAS® software.

7.2. Experimental results

Off-line modeling was first performed, with 200-tap FIR filters, to estimate the transfer functions of the direct secondary paths using an internally-generated white noise to drive the secondary source.

First, the hybrid operation was tested. A two-tone perturbation (1.2 and 2 kHz) in a 40 m/s flow was therefore considered. Fig. 17—where the pressure spectra measured at one of the four error microphones with and without control are plotted—shows the satisfactory behavior of the proposed algorithm. The lowest tone was reduced by 45 dB without any disturbing effect on the higher one, which remained intact. The two tones were estimated via the frequency detection system and a test was run on the resultant values to determine the correct frequency for ALE control.

The multi-tone track and control algorithm behaved just as well with more advanced perturbations. Fig. 18 illustrates waterfall plots at one of the four error sensors for two different excitations in flow, which were two tones (1 and 1.5 kHz) with a 20 m/s flow velocity in Fig. 18(a) and an unidirectional linear sweep (10 Hz/s) with

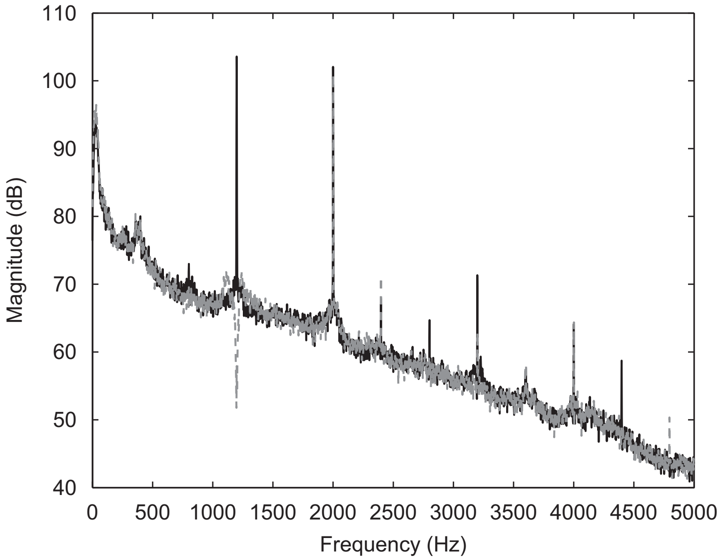

Fig. 17. Validation of the hybrid functioning (solid line: without control; dashed line: with control).

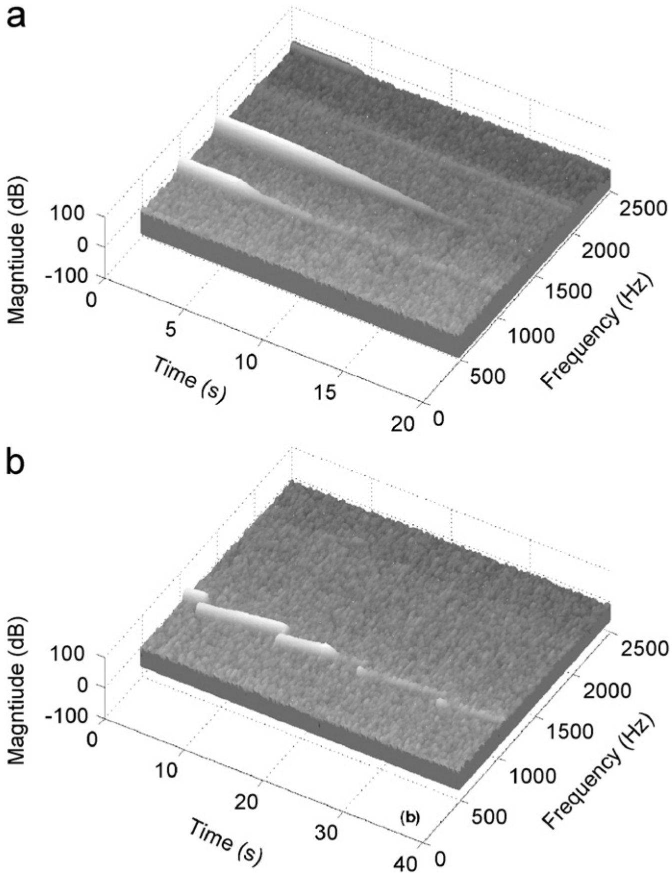

Fig. 18. Validation of the proposed algorithm coupled with self-adaptive ALEs for various excitations: (a) two-tone excitation (control on at 4 s), and (b) chirped excitation (control on at 20 s).

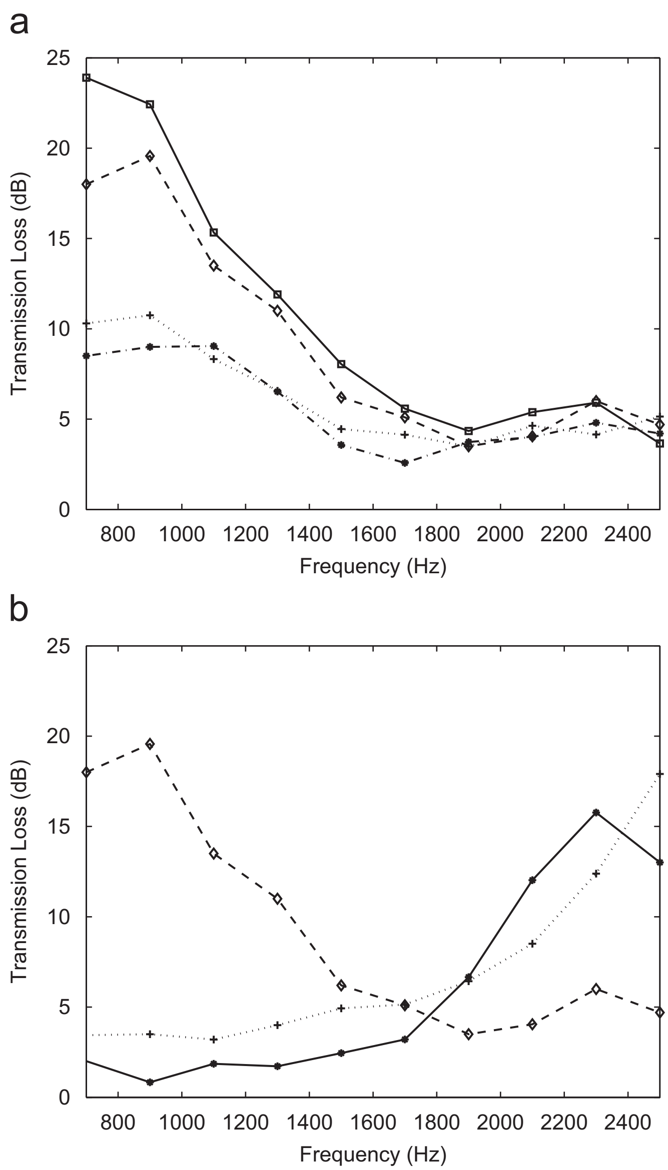

Fig. 19. Influence of various parameters on the TLs: (a) flow velocity and number of hybrid cells (+: 2 hybrid cells $v = 0\,\mathrm{m/s}$; $\star$: 2 hybrid cells $v = 40\,\mathrm{m/s}$; $\square$: 4 hybrid cells $v = 0\,\mathrm{m/s}$; $\diamond$: 4 hybrid cells $v = 40\,\mathrm{m/s}$), and (b) liner type for $v = 40\,\mathrm{m/s}$ (+: honeycomb configuration; $\star$: passive operation of 4 hybrid cells; $\diamond$: active operation of 4 hybrid cells).

a 40 m/s flow velocity in Fig. 18(b). Control started at 4 s and shortly after 20 s, respectively. The controlled signals fell off in the flow noise. These attenuations were obtained with eighth-order control filters, which seemed to offer the best compromise between good reduction and fast convergence.

Lastly, tests were carried out with different flow velocities up to 50 m/s and different numbers of cells, in order to evaluate the far-field impact. The resulting TLs, as well as those coming from measurements carried out in passive mode, are plotted in Fig. 19. Fig. 19(a) accounts for the influence of flow velocity and number of active cells on performance while Fig. 19(b) allows behaviors in passive and active operations to be compared.[1] The noise reduction of the hybrid absorber is also compared to that of a classical liner (wire mesh on a honeycomb structure) of comparable thickness.

[1]Fig. 19(b) just shows the TL obtained with a 40 m/s flow velocity, but the conclusion applies to each velocity.

Thus, it is preferable to consider hybrid cells in large numbers to achieve good noise reduction at low frequencies. The effect of flow velocity is especially felt at low frequencies. ANC is worthwhile up to the cut-off frequency of 1.8 kHz, which is in good agreement with the theoretical predictions developed by Sellen et al. [11]. The passive treatment takes over at higher frequencies. The proposed hybrid liner outperforms the honeycomb configuration. Thus, concerning the aforementioned two-tone excitation (1.2 and 2 kHz), the far-field noise reductions obtained are about 12 dB at 1.2 kHz and 9 dB at 2 kHz.

8. Conclusion

This paper summarizes the design and development of the active part of the proposed new acoustic hybrid passive/active absorber. The use of a piezo-electric actuator enabled an efficient and compact secondary source to be achieved. Pressure reduction was obtained over the whole cross-section of the hybrid cell thanks to optimized positioning of the ceramic. Concerning the controller, a novel algorithm allowing digital adaptive MIMO feedback control is proposed. Bandpass filters counteracting the potential instabilities are implemented to perform ANC independently, cell by cell. Effectiveness depends on the predictability of the noise to be controlled. Thus, the controller can process multi-tone perturbations easily and economically: i.e. with few coefficients.

Next, a time-varying frequency tracking system is presented. Its structure allows the bandpass filters to be rendered self-adaptive, and its implementation in the proposed multi-tone ANC algorithm proved particularly satisfactory. Indeed, it appears that detection disturbed neither control nor even convergence time. The final result is a fully adaptive system that requires very few inputs, which is a decisive advantage for implementation on DSP cards.

Combining both the active and passive operations allows the design of a thin absorber able to achieve significant noise reduction throughout the whole frequency range, for different flow velocities and on large active surfaces. Thus we get between 5 dB and nearly 25 dB reduction in the Matisse flow duct, for velocities up to 50 m/s with a treated area 220 mm long by 55 mm wide. These results are very promising because they show that global control through adaptation of boundary conditions is possible and efficient. Active control is not affected by the flow, thanks to the protecting effect of the wire mesh. The proposed algorithm allows the development of larger active surfaces, necessary to obtain significant noise reduction in industrial applications. Further experiments will be carried out to this end.

Acknowledgment

This work has been supported by the European Community under the SILENCE(R) project (significantly lower community exposure to aircraft noise, GRD1-2000-25297).

References

[1] N. Sellen, M.A. Galland, M. Cuesta, Noise reduction in a flow duct: implementation of a passive/active solution, Journal of Sound and Vibration, 297(3–5) (2006) 492–511.
[2] D. Guicking, K. Karcher, M. Rollwage, Coherent active methods for applications in room acoustics, Journal of the Acoustical Society of America 78 (1985) 1426–1434.
[3] F. Orduna-Bustamante, P.A. Nelson, An adaptive controller for the active absorption of sound, Journal of the Acoustical Society of America 91 (1992) 2740–2747.
[4] T.R. Howard, V.K. Varadan, X. Bao, V.V. Varadan, Piezocomposite coating for active underwater sound reduction, Journal of the Acoustical Society of America 91 (1992) 823–831.
[5] G.C. Nicholson, P. Darlington, Smart surfaces for building acoustics, Proceedings of the Institute of Acoustics 13 (1991) 155–164.
[6] M. Furstoss, D. Thenail, M.A. Galland, Surface impedance control for sound absorption: direct and hybrid passive/active strategies, Journal of Sound and Vibration 203 (2) (1997) 219–236.
[7] H.F. Olson, E.G. May, Electronic sound absorber, Journal of the Acoustical Society of America 25 (1953) 1130–1136.
[8] D. Guicking, E. Lorenz, An active sound absorber with porous plate, Journal of Vibration and Acoustics 106 (1984) 389–392.
[9] M.A. Galland, P. Souchotte, P. Ladner, T. Mazoyer, Experimental investigation of noise reduction in a flow duct through hybrid passive/active liner, Seventh AIAA/CEAS Aeroacoustics Conference, Maastricht, The Netherlands, 28–30 May 2001, AIAA Paper 2001-2221.

[10] O. Hilbrunner, M.A. Galland, N. Sellen, J. Perisse, Optimisation of a hybrid acoustic liner for noise reduction of engine aircraft nacelles, Proceedings of ACTIVE 2002—The 2002 International Symposium on Active Control of Sound and Vibration, vol. 1, Southampton, UK, 2002, pp. 657–668.
[11] N. Sellen, M. Cuesta, M.-A. Galland, Passive layer optimization for active absorbers in flow duct applications, Ninth AIAA/CEAS Aeroacoustics Conference, Hilton Head, South Carolina, 12–14 May 2003, AIAA Paper 2003-3186.
[12] B. Mazeaud, M.-A. Galland, N. Sellen, Design of an adaptive hybrid liner for flow duct applications, 10th AIAA/CEAS Aeroacoustics Conference, Manchester, UK, 10–12 May 2004, AIAA Paper 2004-2852.
[13] M. Morari, E. Zafiriou, Robust Process Control, Prentice-Hall, Englewood Cliffs, NJ, 1989.
[14] S.J. Elliott, Signal Processing for Active Control, Academic Press, New York, 2000, pp. 132–136.
[15] B. Rafaely, S.J. Elliott, Adaptive internal model controller—stability analysis, in: Proceedings of INTER-NOISE'96 Conference, Liverpool, UK, 1996, pp. 983–988.
[16] S.M. Kuo, D.R. Morgan, Active Noise Control Systems, Wiley, New York, 1996, pp. 306–308.
[17] S.J. Elliott, Signal Processing for Active Control, Academic Press, New York, 2000, pp. 289–302.
[19] S.J. Elliott, Signal Processing for Active Control, Academic Press, New York, 2000, pp. 306–319.
[20] S.M. Kuo, D.R. Morgan, Active Noise Control Systems, Wiley, New York, 1996, pp. 200–204.
[21] E. Leboucher, P. Micheau, A. Berry, A. L'Espérance, A stability analysis of a decentralized adaptive feedback active control system of sinusoidal sound in free space, Journal of the Acoustical Society of America 111 (1) (2002) 189–199.
[22] P.A. Regalia, Adaptive IIR Filtering in Signal Processing and Control, Marcel Dekker Inc., New York, 1995, pp. 554–599.
[23] P.A. Regalia, S.K. Mitra, P.P. Vaidyanathan, The digital allpass filter: a versatile signal processing building block, Proceedings of the IEEE 76 (1) (1988) 19–37.
[24] B. Widrow, S.D. Stearns, Adaptive Signal Processing, Prentice-Hall, Inc., Englewood Cliffs, NJ, 1985.
[25] N.K. M'Sirdi, H.A. Tjokronegoro, Cascaded adaptive notch filters: an RML estimation algorithm, in: Proceedings of EUSIPCO 1988, Grenoble, France, 1988, pp. 1409–1412.
[26] J.M. Travassos-Romano, M. Béllanger, Fast adaptive notch filtering in the cascade form, in: Proceedings of EUSIPCO 1988, Grenoble, France, 1988, pp. 567–569.
[27] S. Haykin, Adaptive Filter Theory, second ed., Prentice-Hall International Editions, Englewood Cliffs, NJ, 1991, pp. 477–504.
[28] J.M. Travassos-Romano, M. Béllanger, Fast least squares adaptive notch filtering, Correspondence of the IEEE Transactions on Acoustics, Speech and Signal Processing 36 (9) (1988) 1536–1540.
[29] S. Kim, Y. Park, Active control of multi-tonal noise with reference generator based on on-line frequency estimation, Journal of Sound and Vibration 227 (3) (1999) 647–666.